IEEE Access
Multidisciplinary | Rapid Review | Open Access Journal

Received 21 June 2023, accepted 4 July 2023, date of publication 12 July 2023, date of current version 21 July 2023.

Digital Object Identifier 10.1109/ACCESS.2023.3294565

APPLIED RESEARCH

Development of Hardware-in-the-Loop Simulation for CubeSat Platform: Focusing on Magnetometer and Magnetorquer

HANJOON SHIM[1,2], O-JONG KIM[3], MINHUCK PARK[4], MINKYU CHOI[5], AND CHANGDON KEE[1,2], (Member, IEEE)

[1]Department of Aerospace Engineering, Seoul National University, Seoul 08826, South Korea
[2]Institute of Advanced Machines and Design, Seoul National University, Seoul 08826, South Korea
[3]Department of Aerospace Engineering, Sejong University, Seoul 05006, South Korea
[4]GNSS Research and Development Center, Danam Systems Inc., Anyang 13930, South Korea
[5]Device Solutions Division, Samsung Electronics, Hwaseong 18448, South Korea

Corresponding author: Changdon Kee (kee@snu.ac.kr)

This work was supported by Future Space Navigation & Satellite Research Center through the National Research Foundation funded by the Ministry of Science and ICT, the Republic of Korea (2022M1A3C2074404), contracted through by the Institute of Advanced Aerospace Technology at Seoul National University. The Institute of Engineering Research at Seoul National University provided research facilities for this work.

ABSTRACT This study is aimed at addressing the practical challenges of conducting hardware-in-the-loop simulation (HILS) for a CubeSat attitude determination and control system (ADCS) with a magnetometer and magnetorquer. The inherent problem of magnetometer time-varying bias is typically addressed using compensation methods. Because compensation is performed in orbit, the application of such methods to HILS is difficult. In addition, the magnetorquer has limited applicability to HILS if only magnetorquers without reaction wheels or control moment gyroscopes are used. In general, HILS for CubeSat uses air bearing; however, it cannot be applied to a solely magnetorquer-based ADCS owing to the inertial moments and center of gravity effects induced by the air bearing table. To overcome these challenges, in this study, the magnetometer reliability is enhanced by compensating for temperature, current, and iron effects, which are modeled experimentally, in the pre-launch stage. Then, a novel single axis-based HILS for CubeSats is developed to minimize the disturbances by the ground environment. The torque limit of the magnetorquer is supplemented through a magnetic field generated by a Helmholtz cage. The proposed HILS environment is mathematically modeled to simulate the performance of the CubeSat ADCS, and its reliability is ensured by comparing the simulation with real-time experimental results. To validate the usefulness of the proposed HILS, it is applied to an ADCS based on a low-cost sensor fusion extended-Kalman filter and a linear quadratic regulator controller commonly used in CubeSats. The simulation and experimental results are well matched, demonstrating the potential of the proposed framework.

INDEX TERMS CubeSat, hardware-in-the-loop simulation (HILS), attitude determination and control system (ADCS), magnetometer, time-varying bias, magnetorquer.

I. INTRODUCTION

The hardware-in-the loop simulation (HILS) of the satellite attitude determination and control system (ADCS) is aimed at constructing a simulation loop that includes actual hardware in a real-time embedded system and verifying the integrated system elements. HILS technology has been traditionally used as a satellite ADCS verification technique because it can enable the conduction of tests on various flight scenarios of satellite ADCS in a laboratory that simulates the space environment, thereby increasing the operational reliability of the design system [1]. When verification is performed based on actual hardware through HILS, the conditions for delay, signal noise, non-linear statistical measurements of sensors,

The associate editor coordinating the review of this manuscript and approving it for publication was Agustin Leobardo Herrera-May.

actuator characteristics, and other parameters that were not implemented in the software-in-the-loop simulation (SILS) appear. Therefore, HILS verification based on the actual hardware of the satellite ADCS is necessary to ensure the success of satellite missions [2].

Compared with large-scale satellite projects, the development timeline of CubeSat projects, from design to verification in the development environment, is short. Moreover, the process involves limited resources, facilities, and budget. Consequently, it is challenging to establish space environment simulation equipment and test facilities in the laboratory to perform HILS of the CubeSat ADCS. In addition, certified test equipment that has been used to perform HILS in the space system industry cannot be applied to CubeSat platforms that are lightweight, have a small moment of inertia, and have a small actuator input. Therefore, the verification of the CubeSat ADCS is typically performed through SILS and end-to-end tests, and HILS research on CubeSat platforms has been actively conducted to solve this problem [1], [2], [3], [4], [5], [6], [7], [8], [9].

Notably, the existing HILS devices mainly use air bearings [10], [11], [12], [13], [14]. To this end, it is necessary to use micro air bearings suitable for CubeSat platforms and expend additional efforts to calculate a mathematical model of the external force acting on the test bed for the center of gravity and moment of inertia. This requires the effectiveness of the HILS of the CubeSat ADCS to be evaluated based on functional operation, and it is challenging to demonstrate the reliability of the system through a comparison of ADCS simulation and actual experiment results for the built HILS environment. In addition, small CubeSats, which are classified as nanosatellites weighing 1–10 kg, have limited space for actuator mounting. Because of the space limitations, most CubeSats of 2U or lower adopt a magnetorquer as the only actuator [15]. Because the magnetorquer has small torque input characteristics, the center of gravity shifts or the moment of inertia of the existing test bed may act as a large disturbance factor [7]. In order words, the performance analysis of the weak torque of the actuator becomes more difficult in the HILS facilities. Furthermore, from the perspective of using actual hardware, the time-varying bias of the magnetic field sensor, which is a well-known problem of CubeSats [16], must be resolved to perform HILS.

This study is aimed at the development of HILS for a CubeSat platform equipped with a low-cost magnetometer and magnetorquer, considering the following aspects: First, considering the characteristics of the CubeSat project, it is necessary to build the HILS environment of the CubeSat platform with an easily accessible device. Second, the system must be able to be verified by installing it on the ADCS using actuators and sensors commonly mounted on CubeSats. In particular, the small input torque of the actuator and influence by the moment of inertia of the HILS devices must be considered. Next, the HILS must be performed through a practical solution for actual hardware by solving the time-varying bias problem of the magnetometer used for attitude determination. Finally, the HILS devices for verifying the ADCS of the CubeSat should be mathematically modeled, and all experimental characteristics verified through HILS must be compared with the simulation results to demonstrate its validity. Furthermore, the HILS environment should be configured such that commonly used ADCS algorithms can be applied.

As a key condition for performing HILS, considering the characteristics of actual hardware, we present a solution to the time-varying bias problem of the magnetometer. The time-varying bias issue that occurs in magnetometer measurements was analyzed through experimental compensation, and the statistical characteristics of the measurements were reflected in the attitude determination algorithm.

Next, the HILS construction method is simplified. To this end, a single-axis-based HILS environment is constructed by hanging the CubeSat onto a string so that any developer can easily access it. The performance of the applied ADCS algorithm was verified using a proposed HILS with only a magnetorquer on the ground environment. The accuracy of the designed attitude-determination algorithm, which employs a low-cost magnetometer sensor, was verified simultaneously with the ground verification of the designed controller. Also, considering that the torque of the magnetorquer was very weak, the performance of the proposed method was verified using a Helmholtz cage. The magnetic field generated in the Helmholtz cage was perpendicular to the axis, helping point the magnetic field for attitude determination and verify the single axis control performance of the CubeSat. Here, the magnetic field was set to be three times the size of the magnetic field of the LEO, which amplifies the control input torque, thereby reducing the influence of ground disturbance. By modeling the dominant disturbance torque applied to the CubeSat suspended on a string with a single axis, the ADCS performance was compared and analyzed by performing a simulation.

All the proposed methods have the advantage of effectively compensating for the magnetometer time-varying bias, which has been a chronic problem in CubeSat, and effectively verifying the ADCS algorithm on the ground and analyzing its performance. To confirm the usefulness of the proposed method, experimental compensation of the magnetometer and HILS was performed using SNUGLITE-I engineering model (EM), which is 1.9kg 2U size CubeSat [17], and the results were analyzed.

The remaining paper is organized as follows: Section II describes the ADCS and magnetic field compensation method used in existing CubeSats. Section III describes the proposed time-varying bias solution method for the magnetic field sensor. Section IV describes the commonly used ADCS algorithms that are verified using the HILS. Section V describes the proposed single-axis ADCS HILS configuration and experimental results.

II. AN EXISTING CubeSat ATTITUDE DETERMINATION AND CONTROL SYSTEM

CubeSat ADCSs, which perform active three-axis attitude control, have been developed for radio communication and scientific missions using combinations of thrusters, reaction wheels, magnetorquers, and other actuators [15], [18]. The three-axis active attitude control is performed based on the estimated attitude provided by the attitude determination algorithm.

It is well known that a star tracker, which is the most commonly used device for attitude determination, can estimate satellite attitudes precisely at the arcsec level [19], [20]. However, building an attitude determination sensor for CubeSats is relatively expensive, which is unsuitable considering the budget of the CubeSat project for educational purposes. In addition, arcsec-level accuracy is not required to perform missions for educational purposes, and it is difficult to verify star tracker without simulator in the laboratory. Therefore, in general, CubeSat attitude determination utilizes the on-board MEMS sensor fusion method [21]. It is well known that TRIAD or QUEST vector estimation attitude determination [22] can be achieved easily. Based on this algorithm, techniques such as using a Kalman filter (KF) combining a magnetometer, sun sensor, gyroscope, and other measurements have been proposed [23], [24], [25], [26], [27], [28], [29]. In the case of a LEO satellite, the geomagnetic vector and sun vector are the main indicators of direction for references, including the International Geomagnetic Reference Field (IGRF) model [30] and NASA Jet Propulsion Laboratory sun model [31].

For the attitude determination, magnetometers have been used as critical indicators that can always be employed in LEO satellites [32]. In particular, because CubeSats cannot mount many sensors in a limited physical space, the magnetometer is vital for attitude determination, and its measurement quality significantly affects its performance [33]. However, magnetometer measurements experience time-varying bias because the components are densely arranged in a very small space in the CubeSat, and the magnetometer is mounted in the middle of the on-board area. Many commercial products adopt a tip or boom structure that prevents the distortion of measurement values by moving the magnetometer away from the CubeSat body [34]. However, to adopt this structure, an additional magnetometer deployment device must be designed and added, which is not suitable for CubeSats with insufficient space. In addition, environmental factors must be considered because these devices include the risk of deployment failure and move away from the satellite body.

To overcome the above-mentioned problems, solutions for the time-varying bias of the magnetometer of the CubeSat have been proposed, but they are limited to on-orbit compensation [16], [35], [36]. To date, only a few methods have been proposed to compensate for CubeSat magnetometers before launch. Recursive magnetometer calibration algorithms have been proposed that combine attitude as the most effective way to compensate for the magnetic field sensor on-orbit. The methods listed reduce the measurement error for time-varying bias using a KF [37], [38], extended Kalman filter (EKF) [35], or unscented Kalman filter (UKF). However, these methods require a complex filter design and are compensated for under the assumption that the satellite attitude is known. Therefore, they cannot be applied to CubeSats, where a magnetometer is used as the main indicator to determine the attitude. Methods of compensating the magnetometer independently of attitude have also been proposed [39], [40]; however, their application to CubeSats is limited as on-orbit data must still be received and a recursive algorithm must be applied.

As is well known, CubeSats exhibit an angular velocity of up to 30 deg/s upon ejection from the poly picosatellite orbital deployer (P-POD) [41]. The reliability of the angular velocity estimate is affected by the gyroscope bias, necessitating the use of the magnetometer's rate of change during the initial angular velocity stabilization phase. If magnetometer compensation is to be carried out in orbit, it is necessary to review the performance of the initial operational system, including detumbling control, power generation, communication, and operating methods. Furthermore, guaranteeing the accuracy of compensated results using on-orbit, attitude-independent methods in a CubeSat equipped with limited sensors presents significant challenges [33]. These compensation methods are not applicable for performing HILS in the pre-flight stage. To ensure the reliability of CubeSat's subsystem for short-term missions, it is recommended to enhance the potential for success through preliminary ground testing and conduct tests that predict possible in-orbit events [42]. Therefore, to determine the orientation of the CubeSat using the magnetometer as the main indicator, it is crucial to check the characteristics of the CubeSat magnetometer in advance and prepare a solution for the time-varying bias.

Next, for the attitude control, several methods have been introduced for the CubeSat case using a combination of reaction wheels and magnetorquers. The reaction wheel is suitable for performing attitude control of the CubeSat. However, due to space limitations, most CubeSats of 2U or lower use a magnetorquer as the only actuator [15]. Unfortunately, when using only a magnetorquer, this system is nonlinear time-invariant owing to the continuously changing geomagnetic field in a LEO. Depending on the geomagnetic field, the control torque calculated in the magnetorquer generates an exceedingly small force compared to other actuators. Also, three-axis magnetorquer decoupled each other to calculate the torque according to the cross product between the dipole moment and geomagnetic field. Therefore, for three-axis active attitude control using only the magnetorquer, the aforementioned problem must be addressed.

There are studies on three-axis attitude control algorithms for CubeSats using only a magnetorquer. The PD controller, which is generally used as a satellite attitude control

algorithm, has been used in CubeSats. However, this method requires an input transformation matrix due to decoupled inputs and gain selection, which typically relies on empirical method [43]. In other ways, infinite-horizon, finite-horizon, and constant-gain controllers based on a linear time-varying system that solves the Lyapunov equation [44], [45] have been introduced. To solve the changing geomagnetic field problem, the geomagnetic field was considered to be periodic and included in the linearized model of the spacecraft. Fuzzy [46], predictive [47], and sliding-mode control [48] methods have also been proposed for the magnetorquer control problem in LEO. These methods have been attempted to be applied to the CubeSat platform as innovative strategies. However, in general, the most intuitive method to solve the magnetorquer decoupled problem is to use a linear quadratic regulator (LQR) controller [23], [49], [50], [51].

In this study, a widely used CubeSat ADCS algorithm is applied, which can be verified using the proposed HILS method. The objective is to simplify the ADCS verification process by adopting an easily accessible algorithm while leveraging existing methods. To this end, we first estimate the attitude and angular velocity of the CubeSat by using the EKF as the attitude determination algorithm. The EKF combines measurements from a sun sensor, gyroscope, and magnetometer that compensates for statistical errors caused by time-varying bias. Also, in this study, as the well-known attitude control algorithm, a linear quadratic regulator (LQR) controller was designed. The control states include the Euler angles, angular velocity, and gyroscope bias. The actuator is equipped with PCB-integrated magnetorquers to perform 3-axis active attitude control.

Notably, in the case of the existing on-orbit compensation method, the time-varying bias problem of the magnetometer used in the adopted ADCS cannot be applied to HILS performed pre-launch. Therefore, we establish a new compensation method for the time-varying bias of a magnetometer that can be verified on the ground. The time-varying bias of the magnetometer was divided into temperature, current, and iron effects, and each time-varying bias was experimentally modeled and compensated for before the measurement update of the attitude determination algorithm. The three factors considered in this paper, influencing the magnetometer appear prominently owing to the characteristics of CubeSats because the parts are densely arranged in a very small space.

III. COMPLETE SOLUTION FOR MAGNETIC MEASUREMENT DISTORTION

A. TEMPERATURE COMPENSATION

In general, MEMS sensor measurements are affected by temperature. In particular, in a space environment, the temperature changes significantly depending on the presence or absence of the sun. For a gyroscope, which is the MEMS sensor mounted on the CubeSat, the influence of temperature is reflected by estimating the bias as an attitude determination algorithm state of the EKF, because it is difficult to model the bias change with respect to the temperature in a gyroscope. In addition, low-cost MEMS gyros used in CubeSats are more efficient in estimating bias than in modeling because of their instability. However, the well-known fluxgate-type magnetometer changes depending on temperature [52]. Therefore, the influence of the temperature compensation of the magnetic field measurement B^T_{meas} at the current temperature T can be easily distinguished by a function of the temperature scale factor $s(T)$. At the current temperature, the magnetometer measurements for a reference temperature T_0 can be expressed as Eq. (1):

$$B^T_{meas} = s(T)B^{T_0}_{temp} \tag{1}$$

Here, the scale factor at the current temperature can be expressed by Eq. (2), assuming a first-order linear model:

$$s(T) = s_0 + s_1 T \tag{2}$$

Rewriting Eqs. (1) and (2), the temperature-compensated magnetometer measurement can be expressed by Eq. (3):

$$B^{T_0}_{temp} = \frac{B^T_{meas}}{s_0 + s_1 T} \tag{3}$$

To obtain the scale factors of the magnetometer model coefficients for the temperature, the CubeSat was placed in a clean booth. If a thermal vacuum chamber, which is the best apparatus for temperature change assessment, is utilized, the magnetometer measurements will be affected by the mechanical operation of the chamber. Thus, thermally varying magnetic data collection was conducted in a place where the influence of the magnetometer is as small as possible. The temperature sensor attached next to the sensor was used as the reference temperature because the magnetometer did not provide temperature measurements. In this study, a temperature in the range of 10–30 °C was modeled by changing the clean booth temperature, and the modeling temperature range was referred to for the on-orbit case of the inner products of the CubeSat [17], [53]. Next, to analyze the effect of the magnetometer on the temperature, the bias effect in the static state was checked. Because it was placed in a static environment, the influence of external factors other than the temperature change on the measurements could be neglected. At this time, the reference temperature was set to 25 °C, adopting the datasheet reference temperature of the magnetometer. The scale factor could easily be calculated using the least-squares method by constructing Eq. (4) from Eq. (3) for the kth collected magnetometer and temperature data:

$$\begin{bmatrix} s_0 \\ s_1 \end{bmatrix} = \frac{1}{\hat{B}^{T_0}_{temp}} \begin{bmatrix} 1 & T(t_1) \\ 1 & T(t_2) \\ \vdots & \vdots \\ 1 & T(t_k) \end{bmatrix}^+ \begin{bmatrix} B^T_{meas}(t_1) \\ B^T_{meas}(t_2) \\ \vdots \\ B^T_{meas}(t_k) \end{bmatrix} \tag{4}$$

Here, superscript + indicates a pseudoinverse matrix, and the magnetometer estimate for the reference temperature was calculated using the least-squares method for the collected

magnetic field for each axis and temperature data. The scale factors calculated using Eq. (4) are listed in Table 1.

TABLE 1. Temperature scale factor for each axis.

Scale Factor	X	Y	Z
$s_0[-]$	1.11	1.07	1.08
$s_1[-]/[^\circ C]$	-4.33×10^{-3}	-2.73×10^{-3}	-3.03×10^{-3}

The coefficients are presented in Table 1, and the compensated results using the verification dataset are presented in Fig. 1. In Fig. 1, the bias of the magnetometer changes according to the temperature. And the result shows that the magnetometer measurement in the temperature domain can be modeled linearly. Thus, it can be confirmed that the bias component is removed, only noise remained, and the time-varying bias is stable with respect to the reference temperature.

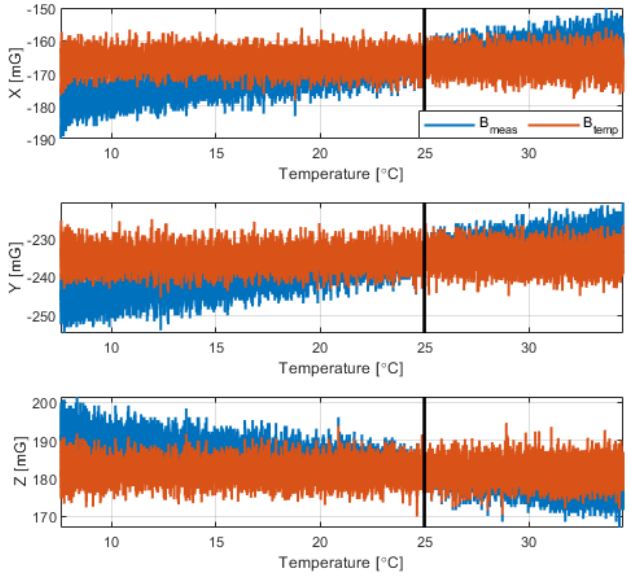

FIGURE 1. Time-varing bias due to temperature variation. The blue and red lines indicate the measurements before and after compensation, respectively. The reference temperature is 25 °C.

B. CURRENT COMPENSATION

The arrangement of the components concentrated in CubeSats causes magnetic field interference between the internal circuits [16], because a magnetic field is generated by the current flowing in the circuit. In this study, it was found that the current flows through the internal circuit, especially when charging through the solar panel in the EPS where the largest current flows, and the current appears the most prominently. The distortions in the magnetometer measurements generated during charging in the integrated CubeSat are depicted in Fig. 2. As shown in Fig. 2, when the current flows through the EPS and solar panels due to sunlight, distortion of the magnetic field measurements occurs. This measurement distortion phenomenon is caused by a magnetic field generated by the current flowing in the EPS internal circuit charged by sunlight from the solar panels. This bias change must be removed in advance to reduce the statistical uncertainty of attitude determination algorithm measurements.

Therefore, in this study, the idea is that the magnetic field generated by the current is the same as that of a wire with an electronic circuit fixed to the CubeSat internal body came into focus. The magnetic field generated by the current can be defined using the Biot–Savart law, as shown in Eq. (5). Because the magnetometer attached to the CubeSat and the wire flowing inside the EPS are fixed, the three-axis magnetic field generated by the current vector $\mathbf{i}$ can be simplified.

$$\delta\mathbf{B}(\mathbf{i}) = \frac{\mu_0 \mathbf{i}}{4\pi}\int \frac{d\ell \times \hat{r}}{r^2} \approx \mathbf{K}_e \cdot \mathbf{i} \tag{5}$$

$$\delta\mathbf{B} = \begin{bmatrix} \delta B_x & \delta B_y & \delta B_z \end{bmatrix}^T,$$

$$\mathbf{K}_e = \begin{bmatrix} K_e^{11} & K_e^{12} & K_e^{13} \\ K_e^{21} & K_e^{22} & K_e^{23} \\ K_e^{31} & K_e^{32} & K_e^{33} \end{bmatrix},$$

$$\mathbf{i} = \begin{bmatrix} i_x & i_y & i_z \end{bmatrix}^T \tag{6}$$

Here, μ_0 represents the permeability of free space, $d\ell$ represents a vector line element of the current direction, r represents the distance from $d\ell$, and $\hat{r}$ represents a unit vector in the direction of r.

In other words, the magnetic field phenomenon caused by the current can be interpreted as being expressed as a magnetometer measurement $\mathbf{B}_{meas}^{curr}(\mathbf{i})$ obtained by adding a reference $\mathbf{B}_0$ and a current-distorted magnetic field $\delta\mathbf{B}(\mathbf{i})$, which can be written as

$$\mathbf{B}_{meas}^{curr}(\mathbf{i}) = \mathbf{B}_0 + \delta\mathbf{B}(\mathbf{i}) \tag{7}$$

Therefore, by modeling the coefficient K_e from Eq. (6) because of the distortion of the magnetic field with respect to the current, the current-distorted magnetometer measurement can be compensated. Thus, because the current flowing through each axis can be measured by EPS, the magnetic field distortion coefficient of the current can be modeled. The method of modeling the magnetic distortion coefficient owing to the current charged to the EPS through the solar panel proceeds in the following steps.

[Step 1] Prepare a device that can fix the CubeSat and a sunscreen that blocks the entire CubeSat body without one side.

[Step 2] Cover all sides with sunscreen to prevent charging current, and collect magnetometer measurements. The collected measurements are the undistorted reference magnetometer measurements $\mathbf{B}_0$.

[Step 3] As shown in Fig. 3, install a sunscreen to charge only one side of the CubeSat, and collect current $\mathbf{i}$ and magnetic field measurements $\mathbf{B}_{meas}^{curr}$ on that side.

[Step 4] Repeat steps 2 and 3 to collect current and magnetometer data for all solar panel attached surfaces.

[Step 5] From Eq. (7), obtain the magnetic field measurement $\delta\mathbf{B}(\mathbf{i})$ generated by the current using the reference

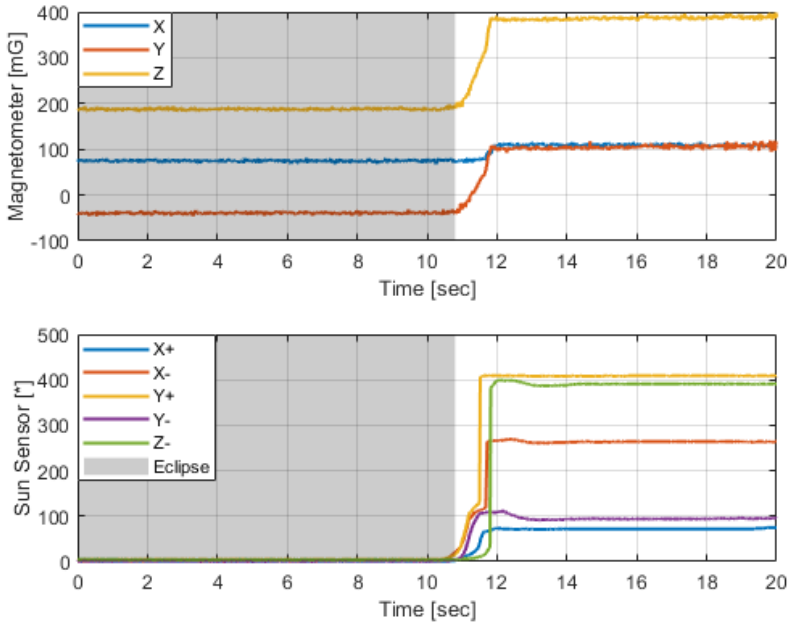

FIGURE 2. Magnetometer measurement distortion when charging solar panels. The upper and lower panels present the magnetic field and photodiode type sun sensor measurements, respectively.

FIGURE 3. Sunscreen and CubeSat cradle for current compensation experiment, which is composed of a screen that exposes one side of the CubeSat and a screen that covers the entire surface.

measurements $\mathbf{B}_0$, current $\mathbf{i}$, and distorted magnetic field measurements $\mathbf{B}_{meas}^{curr}$ collected on each side.

[Step 6] Now, organize all the collected data into a matrix and calculate the magnetic field distortion coefficient due to the current using the least-squares method in Eq. (8). In this case, a more accurate modeling coefficient can be estimated as the number of datasets increases.

$$\mathbf{K}_e = \delta\mathbf{B} \cdot \left[\mathbf{i}^T(\mathbf{i} \cdot \mathbf{i}^T)^{-1}\right] \tag{8}$$

[Step 7] To verify the accuracy of the modeled coefficients, collect the magnetometer distortion for all axes and reference magnetic field measurements.

[Step 8] Compensate the magnetic field measurements that are distorted with respect to the current using modeling coefficients, and compare and verify the results collected in Step 7.

The calculated coefficient is shown in Eq. (9) below:

$$K_e = \begin{bmatrix} 42.21 & 52.54 & -21.79 \\ 5.46 & -134.14 & 474.03 \\ 40.83 & -50.29 & 668.83 \end{bmatrix} \frac{[mG]}{[\mathrm{A}]} \tag{9}$$

Checking the coefficients calculated above confirms that the magnitudes of the coefficients in the second and third columns of the matrix are relatively large, which can be interpreted as the current being distorted more in the Y- and Z-axis directions. In particular, because the coefficient in the Z-axis direction is the largest, the electronic circuit of the CubeSat generates a magnetic field in the corresponding direction. To verify the results calculated above according to Steps 7 and 8, the distorted magnetic field measurements and compensation results for the current flowing through the solar panel on each axis are provided in Fig. 4. As shown in Fig. 4, even if the current changes, the distortion of the magnetometer measurement remains at a certain level. This approach is an ingenious way to model experimentally the time-varying bias of magnetic-field measurements, which has been a chronic problem in CubeSats. The residual error for current compensation is presented in Table 2 and is considered a characteristic of magnetic field sensor measurements.

C. HARD- AND SOFT-IRON CALIBRATION

Owing to the arrangement of the integrated components in the CubeSat, the magnetic field sensor has another problem caused by the metal. Magnetic field distortion occurs due to the metallic material of the CubeSat. The influence of iron on

TABLE 2. Current compensation measurement residual error.

RMSE	X $[mG]$	Y $[mG]$	Z $[mG]$
Before	13.87	45.31	98.28
Proposed method (Current compensated)	4.60	7.59	8.28

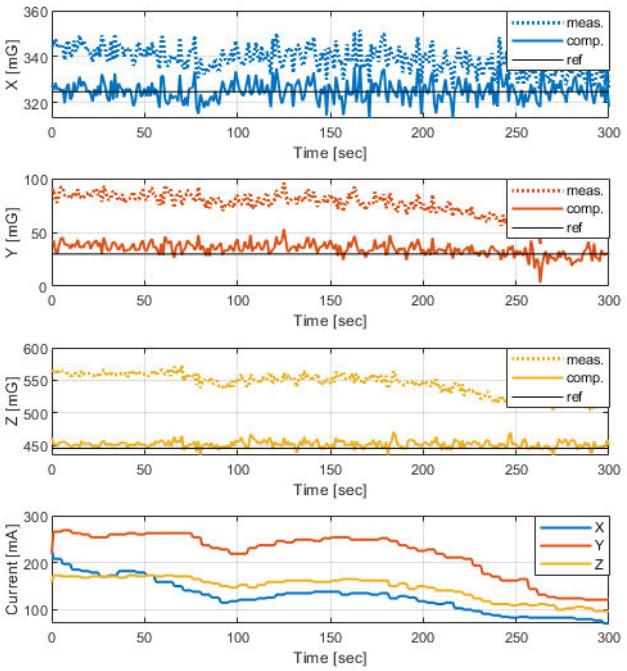

FIGURE 4. Current compensation results in time domain at each axis: the result of before/after compensation of the magnetic field measurement of each axis, and the reference measurement is collected when all CubeSat surfaces are covered.

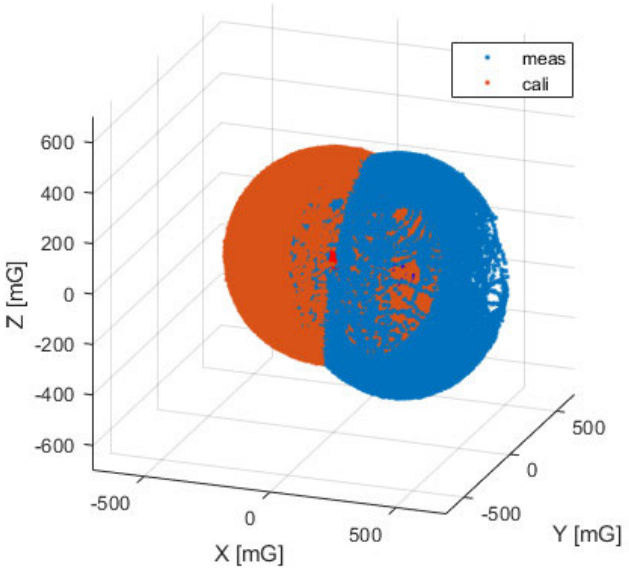

FIGURE 5. Hard- and soft-iron calibration results in the magnetic field domain.

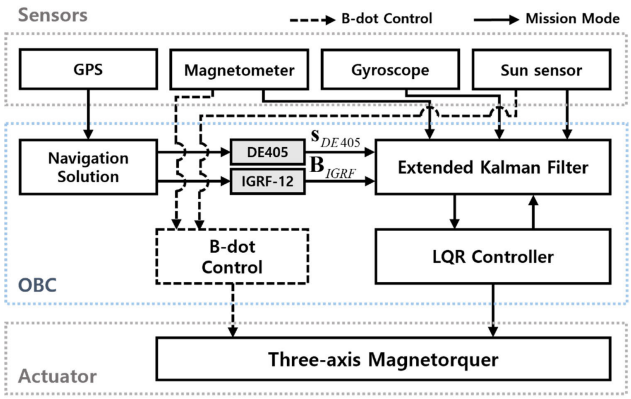

FIGURE 6. Overall block diagram of ADCS.

magnetometers is well known mainly from strapdown-type magnetic field sensor calibration for aircraft [54], [55]. The effects of metals can be divided into two types. The first is the hard iron effect, which causes an offset error in the magnetic field measurements. The second is the soft iron effect, which causes distortion of the uniformity of the geomagnetic field in all directions, i.e., the ellipsoid error. An ellipsoidal calibration method was utilized to eliminate these errors. The magnetic field measurements employed for ellipsoid compensation use temperature- and current-compensated measurements.

Data collection for performing hard- and soft-iron calibrations of the magnetometer can be conducted in two ways. The first is to use a Helmholtz coil to generate a three-dimensional spherical magnetic field. The second is to collect magnetic field data by directly rotating the CubeSat in an outdoor environment, where the size of the magnetic field is known. The method proposed in this paper is a practical approach that anyone can access, and the data are collected by rotating the CubeSats outdoors. The obtained measurements can yield the true value from the IGRF-12 model. Data were collected for 30 min at 50 Hz, temperature compensation was performed, and data were collected at night when the sun went down to prevent current from flowing.

The results of the magnetometer measurements performed with hard- and soft-iron calibration are shown in Fig. 5. Unlike the results in which the magnetic field was highly biased owing to the arrangement of the parts of the CubeSat, the corrected results are close to a sphere. In this way, by performing temperature and current compensation and magnetic field correction by iron, the time-varying bias of the magnetometer measurements was compensated, and the uncertainty was reduced. The final time-varying bias of magnetometer were considered to be measurement noise in the EKF of attitude determination by reflecting the statistical error.

IV. ATTITUDE DETERMINATION AND CONTROL SYSTEM FOR HARDWARE-IN-THE LOOP SIMULATION

A. OVERALL SYSTEM CONFIGURATION

The entire ADCS system is configured as shown in Fig. 6. To establish a HILS method applicable to a general

CubeSat platform, well-known ADCS hardware and algorithms are adopted and configured. The parts that constitute an ADCS are divided into sensors, an on-board computer, and an actuator. A three-axis MEMS MPU-3300 gyroscope by InvenSense and an HMC5843 low-cost three-axis magnetometer by Honeywell were utilized. Five SLCD-61N8 photodiode-type coarse sun sensors were attached to solar panels on the +x, −x, +y, −y, and −z sides. The dipole momentum of the magnetorquers was approximately 0.038 A·m^2, and three-axis PCB-integrated magnetorquers were integrated into the solar panels along each axis.

When the CubeSat is ejected from the P-POD, momentum is generated from the biased center of gravity of the CubeSat, causing it to rotate at an arbitrary angular velocity. Therefore, immediately after ejection, the B-dot control mode is first implemented to stabilize the angular velocity of the CubeSat. Here, the B-dot controller that decreases the change rate of the magnetic field is designed. When the angular velocity is stabilized within 0.3 deg/s, nadir pointing ADCS is performed. In the mission mode, ADCS is performed using all sensors. GPS navigation solutions provide a position on the orbit, which is used to calculate the reference vector from the magnetic field model (IGRF-12) and solar system model (DE405). By utilizing the reference vectors, the EKF is constructed using measurements from the magnetometer, gyroscope, and sun sensors. The estimated state from the EKF is then provided to the LQR controller and employed for attitude control. The control input calculated by the LQR controller is reflected in the EKF dynamics. The coordinate system used was based on the Earth-centered inertial (ECI) and Earth-centered Earth-fixed coordinate systems, and the radial, in-track, cross-track (RIC) coordinate system was defined as a local frame. The relationship between the coordinate systems is shown in Fig. 7. The sun ephemeris model, which is used for attitude determination, is defined in the ECI, and the magnetic field DE405 model is defined in the north-east-down coordinate system. All reference models are converted into the local coordinate system through the rotation matrix ($C^{\text{to}}_{\text{from}}$) relationship between each coordinate system. The RIC coordinate system defined by the ECI coordinate system is defined as shown in Eq. (10). Here, r and v represent the position and velocity of the satellite, respectively:

$$\hat{e}_1 = \frac{r_{ECI}}{|r_{ECI}|}, \quad \hat{e}_2 = \frac{r_{ECI} \times v_{ECI}}{|r_{ECI} \times v_{ECI}|}, \quad \hat{e}_3 = \hat{e}_2 \times \hat{e}_1 \tag{10}$$

$$C^{Local}_{ECI} = \begin{bmatrix} \hat{e}_3 & -\hat{e}_2 & -\hat{e}_1 \end{bmatrix} \tag{11}$$

B. ATTITUDE DETERMINATION ALGORITHM: EXTENDED KALMAN FILTER

To construct the EKF used for attitude determination, state variables such as those in Eqs. (12)–(15) are considered. The

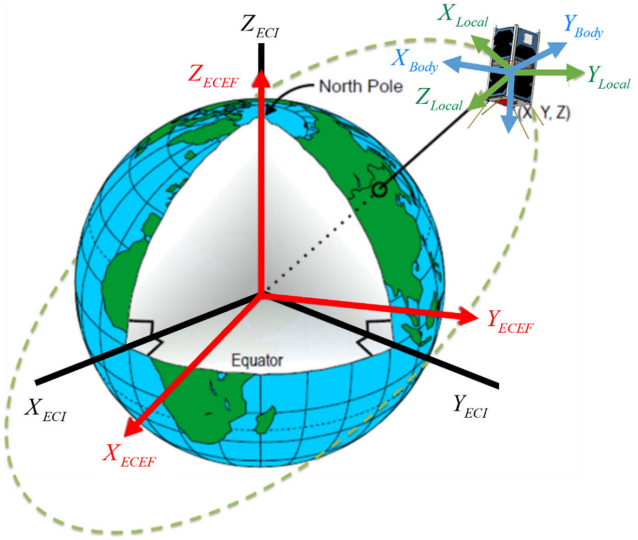

FIGURE 7. Coordinate system used in SNUGLITE-I CubeSat ADCS.

state variables include a quaternion $\mathbf{q}$, angular velocity ω, and angular velocity bias $\mathbf{b}$. The angular velocity is defined in the body frame with respect to the local frame, and the angular velocity bias is a state variable introduced to estimate the unstable bias of the gyroscope:

$$\mathbf{x}(t) = \begin{bmatrix} \mathbf{q} & \boldsymbol{\omega} & \mathbf{b} \end{bmatrix}^T \tag{12}$$

$$\mathbf{q} = \begin{bmatrix} q_0 & q_1 & q_2 & q_3 \end{bmatrix}^T \tag{13}$$

$$\boldsymbol{\omega} = \begin{bmatrix} \omega_x & \omega_y & \omega_z \end{bmatrix}^T \tag{14}$$

$$\mathbf{b} = \begin{bmatrix} b_x & b_y & b_z \end{bmatrix}^T \tag{15}$$

The nonlinear system described for each state variable is composed of Eqs. (16) and (17) [56]:

$$\begin{bmatrix} \dot{\mathbf{q}} \\ \dot{\omega} \\ \dot{\mathbf{b}} \end{bmatrix} = \begin{bmatrix} \frac{1}{2}\Omega(\boldsymbol{\omega})\mathbf{q} \\ \mathbf{J}^{-1}\left(\mu \times \mathbf{B} - \boldsymbol{\omega} \times (\mathbf{J} \cdot \boldsymbol{\omega})\right) \\ \mathbf{0}_{3\times 3} \end{bmatrix} + \begin{bmatrix} \mathbf{0} \\ \boldsymbol{\eta}_{\text{drift}} \\ \boldsymbol{\eta}_{\text{bias}} \end{bmatrix} \tag{16}$$

$$\Omega(\boldsymbol{\omega}) \equiv \begin{bmatrix} 0 & -\omega_x & -\omega_y & -\omega_z \\ \omega_x & 0 & \omega_z & -\omega_y \\ \omega_y & -\omega_z & 0 & \omega_x \\ \omega_z & \omega_y & -\omega_x & 0 \end{bmatrix} \tag{17}$$

where $\mathbf{J}$ is the moment of the inertia tensor of the CubeSat, μ is the magnetorquer vector for the control input, $\mathbf{B}$ is geomagnetic field vector, and $\boldsymbol{\eta}_{drift}$ and $\boldsymbol{\eta}_{bias}$ are the process noise for the system equation.

Next, the equation of the KF described in a nonlinear form is composed of Eqs. (18) and (19), where the disturbance is considered to be Gaussian noise:

$$\dot{\mathbf{x}}(t) = f\left(\mathbf{x}(t), \mathbf{u}(t)\right) + \mathbf{w}(t), \mathbf{w}(t) \sim N(0, Q) \tag{18}$$

$$Q = \begin{bmatrix} \sigma_q^2 I_{4\times 4} & \mathbf{0} & \mathbf{0} \\ \mathbf{0} & \sigma_\omega^2 I_{3\times 3} & \mathbf{0} \\ \mathbf{0} & \mathbf{0} & \sigma_b^2 I_{3\times 3} \end{bmatrix} \tag{19}$$

Here, the process noise $\mathbf{w}(t)$ is assumed to be zero-mean white noise with a variance matrix Q. The covariance matrix Q reflects disturbances that are not modeled in dynamic equations as noise. These values are documented in detail in [57].

Next, Eqs. (20)–(23) are used to define the measurement equation of the Kalman filter. The measurement vector consists of magnetometer $\mathbf{B}_{meas}$, sun sensor $\mathbf{s}_{meas}$, and gyroscope $\boldsymbol{\omega}_{meas}$ measurements. The magnetometer measurements used in this study compensate for the time-varying bias of the magnetometer. The nonlinear measurement equation can be composed of a magnetic field model, solar system model, and estimated angular velocity and bias:

$$\mathbf{z}(t) = h(\mathbf{x}(t)) + \mathbf{v}(t), \mathbf{v}(t) \sim N(0, R) \tag{20}$$

$$\mathbf{z}(t) = \begin{bmatrix} \mathbf{B}_{\text{meas}} & \mathbf{s}_{\text{meas}} & \boldsymbol{\omega}_{\text{meas}} \end{bmatrix}^T \tag{21}$$

$$\begin{aligned} h(\mathbf{x}(t)) &= \begin{bmatrix} \mathbf{B} \\ \mathbf{s} \\ \boldsymbol{\omega} + \mathbf{b} \end{bmatrix} \\ &= \begin{bmatrix} C_{Local}^{Body} C_{ECI}^{Local} C_{ECEF}^{ECI} C_{NED}^{ECEF} \frac{\mathbf{B}_{IGRF}}{|\mathbf{B}_{IGRF}|} \\ C_{Local}^{Body} C_{ECI}^{Local} \mathbf{s}_{DE405} \\ \boldsymbol{\omega} + \mathbf{b} \end{bmatrix} \end{aligned} \tag{22}$$

$$R = \begin{bmatrix} \sigma_{\text{mag}}^2 / |\mathbf{B}_{\text{IGRF}}|^2 I_{3\times 3} & \bar{0} & \bar{0} \\ \bar{0} & \sigma_{\text{sun}}^2 I_{3\times 3} & \bar{0} \\ \bar{0} & \bar{0} & \sigma_{\text{arw}}^2 I_{3\times 3} \end{bmatrix} \tag{23}$$

Here, $\mathbf{B}_{IGRF}$ is the reference vector of the geomagnetic field model (IGRF-12), $\mathbf{s}_{DE405}$ is the reference vector of the sun ephemeris model (DE405), and the symbols of $\sigma_{mag}, \sigma_{sun}$, and σ_{arw} represent measurement noise of the magnetometer, sun sensor, and gyroscope, respectively.

Linearizing the equation given by the definition of EKF leads to Eqs. (24) and (25):

$$\dot{\mathbf{x}} = F\mathbf{x} + G\mathbf{u} + \Gamma\mathbf{w}, \mathbf{w} \sim N(0, Q) \tag{24}$$

$$\mathbf{z} = H\mathbf{x} + \mathbf{v}, \mathbf{v} \sim N(0, R) \tag{25}$$

where F and G in Eq. (24) are the partial derivatives of $f(\mathbf{x}(t), \mathbf{u}(t))$ with respect to $\mathbf{x}$ and $\mathbf{u}$, respectively. Γ is a partial derivative of $\mathbf{w}$ with respect to $\boldsymbol{\eta}$. H in Eq. (25) is the partial derivative of $h(x)$ with respect to state $\mathbf{x}$. $\boldsymbol{\omega}_{EL}^{L}$ refers to the angular velocity at which the local frame changes while orbiting and can be written as $[\,0 \;\; -n \;\; 0\,]^T$.Each matrix used to construct the EKF can be found in described in [58].

C. ATTITUDE CONTROL ALGORITHM: LINEAR QUADRATIC REGULATOR CONTROLLER

To represent attitude as an equation of motion M, we assume that CubeSat is a rigid body and that the body frame is fixed at the center of mass. Because the CubeSat is a rigid body and the center of gravity is assumed to be located at the center of the rectangular parallelepiped, the diagonal component of the moment of inertia becomes zero. Then, the moment for the rotational motion can be written as in Eq. (26) [59], [60]. Here, the disturbance considered in the design of the attitude controller is the gravitational gradient torque τ_{gg} in Eq. (27). In addition, as an input, the control torque τ_{mt} is defined as the cross product of the dipole moment of the magnetorquer and the magnetic field of the earth, as shown in Eq. (28):

$$\begin{aligned} M &= \begin{bmatrix} M_x \\ M_y \\ M_z \end{bmatrix} = \begin{bmatrix} J_x\dot{p} + (J_z - J_y)qr \\ J_y\dot{q} + (J_x - J_z)rp \\ J_z\dot{r} + (J_y - J_x)pq \end{bmatrix} \\ &= \tau_{gg} + \tau_{mt} \end{aligned} \tag{26}$$

$$\tau_{gg} = 3n^2 \begin{bmatrix} (J_z - J_y)\sin\phi\cos\phi\,(\cos\theta)^2 \\ (J_z - J_x)\sin\theta\cos\theta\cos\phi \\ (J_x - J_y)\sin\phi\sin\theta\cos\theta \end{bmatrix} \tag{27}$$

$$\begin{aligned} \tau_{mt} &= \mu \times \mathbf{B} \\ &= \begin{bmatrix} \mu_y B_z - \mu_z B_y \\ \mu_z B_x - \mu_x B_z \\ \mu_x B_y - \mu_y B_x \end{bmatrix} \end{aligned} \tag{28}$$

To introduce the Euler angles ϕ, θ, and ψ as state variables, the body-fixed angular velocities p, q, and r can be expressed using the Euler 3-2-1 transformation relationship, and a small-angle approximation can be assumed to linearize equations as in Eq. (29) [57].

$$\begin{aligned} \dot{p} &\approx \frac{n(J_z - J_y)}{J_x} r + \frac{3n^2(J_z - J_y)}{J_x}\phi + \frac{1}{J_x}\left(\mu_y B_z - \mu_z B_y\right) \\ \dot{q} &\approx \frac{3n^2(J_z - J_x)}{J_y}\theta + \frac{1}{J_y}\left(\mu_z B_x - \mu_x B_z\right) \\ \dot{r} &\approx \frac{n(J_y - J_x)}{J_z} p + \frac{1}{J_z}\left(\mu_x B_y - \mu_y B_x\right) \end{aligned} \tag{29}$$

Here, n represents the mean motion.

Next, the states variables $\mathbf{x}_c$ of the LQR controller are defined as consist of Euler angles and body-fixed angular velocity in Eq. (30). The input variable $\mathbf{u}$ is defined as the control torque calculated from the magnetorquer, as shown in Eq. (31):

$$\mathbf{x}_c = \begin{bmatrix} \phi & p & \theta & \delta q & \psi & r \end{bmatrix}^T \tag{30}$$

$$\mathbf{u} = \tau_{mt} = \begin{bmatrix} u_x & u_y & u_z \end{bmatrix}^T \tag{31}$$

Here, δq is designed as a controller for maintaining the mean motion, which means that the CubeSat maintains the center of the Earth.

The system for constructing the LQR controller is shown in Eqs. (32)–(33):

$$\dot{\mathbf{x}}_c = A_c\mathbf{x}_c + B_c\mathbf{u} \tag{32}$$

where Eq. (33), as shown at the bottom of the next page.

Because the input matrix B_c changes with the geomagnetic field, the control gain is calculated using the following cost functions at each measurement interval. A steady state is assumed to facilitate convenient implementation. The LQR gain solution obtained by solving Eq. (34) is implemented

using the method of Potter [58]:

$$J = \frac{1}{2}\int_0^\infty \mathbf{x}_c(t)^T Q_c \mathbf{x}_c(t) + \mathbf{u}(t)^T R_c \mathbf{u}(t) dt \tag{34}$$

$$K_c(t) = R_c^{-1} B(t)^T P(t),\ \mathbf{u}(t) = -K_c(t)\mathbf{x}_c(t) \tag{35}$$

where P is the solution of the following algebraic Riccati equation:

$$\dot{P}_\infty = 0, A^T P + PA - PBR_c^{-1}B^T P + Q_c = 0 \tag{36}$$

V. A SINGLE AXIS-BASED HARDWARE-IN-THE-LOOP SIMULATION

A. SIMULATION CONFIGURATION

We establish a single-axis-based HILS environment that incorporates twist torque modeling for the string of a hanging CubeSat. Because the system is based on a single axis, the ADCS performance can be intuitively evaluated, and we demonstrate that it is possible to compare and verify actual experimental results and simulations by modeling the twisting torque of the string. The purpose of HILS is that verifying ADCS algorithm in two ways. First, the accuracy of the EKF must be guaranteed by properly compensating for the time-varying bias of the proposed compensation and calibration algorithms. Second, the active control accuracy of the LQR controller should be verified. The Helmholtz cage is used for two purposes: to verify the time-varying bias compensation of the magnetometer, and to minimize the effect of ground disturbance on the small torque force of the PCB-integrated magnetorquer. The objective is to confirm whether time-varying bias compensation is appropriately reflected in the EKF by minimizing the influence of magnetic distortion and to amplify the torque of the magnetorquer that is dependent on the external magnetic field. To this end, SNUGLITE-I CubeSat EM was suspended on a string to simulate a single-axis zero-gravity environment in a clean booth, and real-time ADCS HILS was performed.

The overall configuration of the CubeSat HILS is shown in Fig. 8. The CubeSat is located in the Helmholtz cage, and the HILS control station configures the experiment environment to allow the data to be checked outside the Helmholtz cage. To receive the status data determined through CubeSat in real time, a wireless fidelity (Wi-Fi) module is additionally installed to ensure that data can be transmitted and received wirelessly. The CubeSat consists of all hardware that can perform ADCS verification. The coarse sun sensors, magnetometer, and gyroscope for attitude determination are configured, and the onboard temperature sensor and EPS current sensor are used to implement the proposed magnetometer compensation algorithm. For attitude control, only the magnetorquers included in each axis integrated PCB modules are used.

To simulate the magnetic field and sun used as measurements in the EKF, a halogen lamp was utilized to simulate sunlight, and a Helmholtz cage was employed to simulate the magnetic field. However, unlike in the space environment, inside the ground clean booth, position, time, and velocity information of the GPS navigation solution cannot be provided; therefore, model reference vectors cannot be used from the magnetic field model and sun ephemeris model used in the EKF. To overcome this issue, after fixing the CubeSat with respect to the reference direction, the average measurements of the magnetometer and sun sensor are defined as model vectors of local coordinates, as shown in Eqs. (37) and (38):

$$\mathbf{B}_{IGRF} \triangleq \frac{1}{N}\sum_{k=1}^{N} \mathbf{B}_{meas}(k) \tag{37}$$

$$\mathbf{s}_{DE405} \triangleq \frac{1}{N}\sum_{k=1}^{N} \mathbf{s}_{meas}(k) \tag{38}$$

Next, the following method overcomes the environmental factors of attitude control. The PCB-integrated magnetorquer

$$A_c = \begin{bmatrix} 0 & 1 & 0 & 0 & n & 0 \\ \frac{3n^2(J_z - J_y)}{J_x} & 0 & 0 & 0 & 0 & \frac{n(J_z - J_y)}{J_x} \\ 0 & 0 & 0 & 1 & 0 & 0 \\ 0 & 0 & \frac{3n^2(J_z - J_y)}{J_y} & 0 & 0 & 0 \\ -n & 0 & 0 & 0 & 0 & 1 \\ 0 & \frac{n(J_y - J_x)}{J_z} & 0 & 0 & 0 & 0 \end{bmatrix}$$

$$B_c = \begin{bmatrix} 0 & 0 & 0 \\ 0 & \frac{B_z}{J_x} & -\frac{B_y}{J_x} \\ 0 & 0 & 0 \\ -\frac{B_z}{J_y} & 0 & \frac{B_x}{J_y} \\ 0 & 0 & 0 \\ \frac{B_y}{J_z} & -\frac{B_x}{J_z} & 0 \end{bmatrix} \tag{33}$$

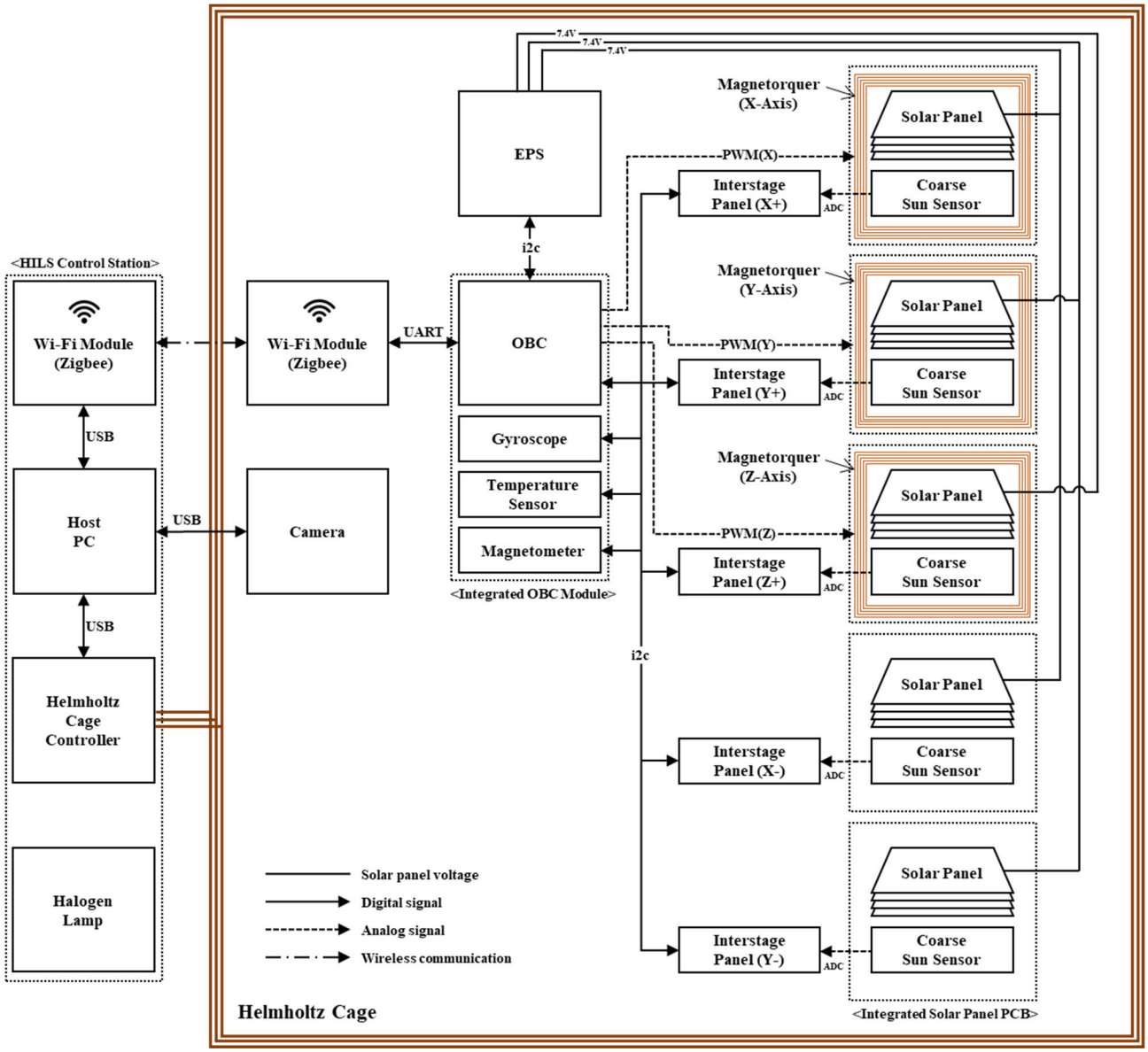

FIGURE 8. Proposed HILS environment system configuration.

equipped with SNUGLITE-I produces very small torques of up to 10^{-6} N·m, making it vulnerable to disturbances in the simulated single-axis zero-gravity environment, and its control performance is difficult to verify. In particular, the twisting torque of the string simulated by the zero-gravity environment of the CubeSat acts as a disturbance because this torque is not modeled in the controller. Therefore, in this study, focusing on the characteristics of the magnetorquer depending on the magnitude of the external magnetic field, we developed a method for verifying the performance of the ADCS algorithm on the ground by improving the control-torque performance with the magnetic field generated by the Helmholtz cage. The proposed single-axis HILS environment is shown in Fig. 9, and the actual built environment using the CubeSat is depicted in Fig. 10. In Fig. 9, the magnetic field generated by the Helmholtz cage is perpendicular to the axis on which the CubeSat is hung, and it is a static vector in which the magnetorquer can apply the maximum force on the X-Y plane. In addition, the control torque defined in Eq. (28) increases with the generated magnetic field by setting it to 1500 mG, which is more than three times the average magnetic field of the earth. By increasing the control torque, the uncertainty of the disturbance factor was reduced and the convergence speed of the ground experiment was improved. Simultaneously, the ADCS data calculated in real time on the CubeSat for the experiment were monitored using the Wi-Fi module.

A single-axis HILS environment was modeled to compare and verify the performance of the ADCS with that obtained in the simulation. This environment works differently from the

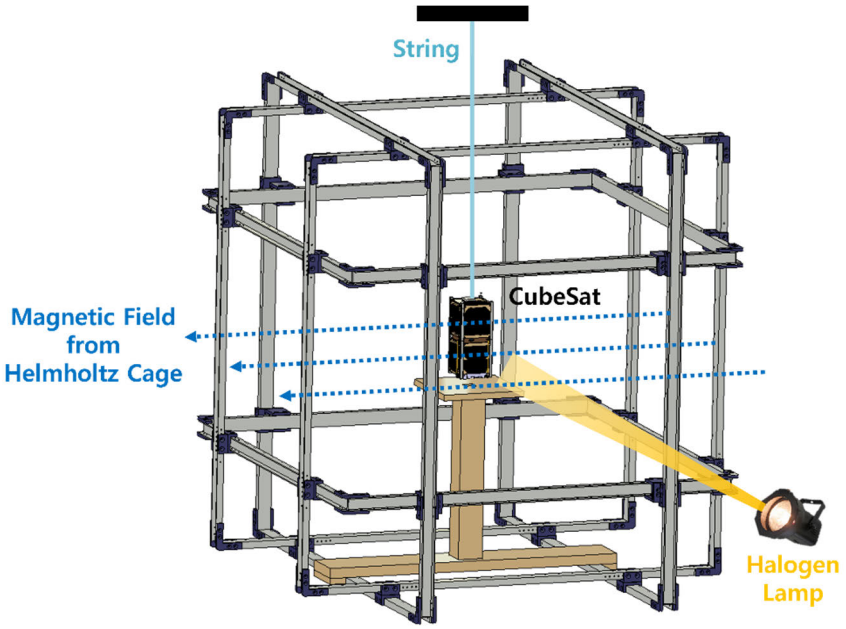

FIGURE 9. Single-axis HILS environment for verification of ADCS. The CubeSat is hung on a string and generates a magnetic field from a Helmholtz cage. Sunlight is simulated by a halogen lamp.

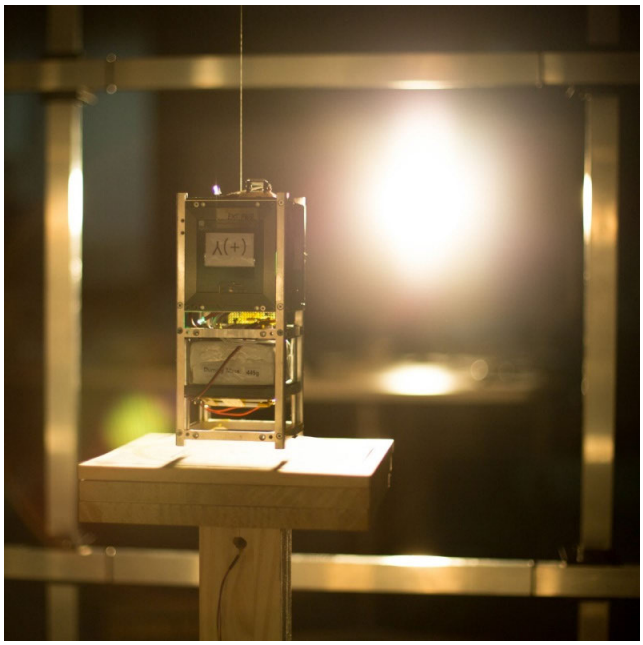

FIGURE 10. HILS environment built using SNUGLITE-I EM.

space environment because of the twisting torque of the string used to hang the CubeSats. This torque can be modeled [61] using Eq. (39):

$$\tau_{str} = \kappa\psi, \ \kappa = 5.76 \times 10^{-8}[N \cdot m/rad] \qquad (39)$$

Here, κ is a constant for the twisted string and is the modeling result of the rotation period after the CubeSat is hung on the string. From Eq. (39), it can be observed that the torque acts in proportion to the rotation angle ψ from the equilibrium point of the string. That is, the external force can be minimized only when the experiment is performed by maintaining the state of rotational equilibrium of the string under the experimental conditions. The torque of Eq. (39) was added to the derived nonlinear equation in Eq. (29) to analyze the simulation results for a single-axis HILS and compare them with the actual experimental results. The HILS results for the proposed method are presented in Figs. 11 and 12. Here, the results are compared between the environments in which the magnetic field is generated using a Helmholtz cage and that in which it was not. The comparative group has the following meaning. First, the controllable magnetic field direction vector is reflected in the update of the EKF measurements. It can be inferred that the statistical error corresponding to the time-varying bias of the magnetometer is well reflected. The second is to propose a ground HILS environment that is not affected by disturbances by amplifying the input torque of the magnetorquer. The environment has many additional disturbance factors compared to space. In particular, the proposed system cannot be vulnerable to disturbances if a small input actuator is used as a PCB-integrated magnetorquer. To prove this point, the amplified and non-amplified magnetic fields from the Helmholtz cage were compared.

B. SIMULATION RESULT

As shown in Fig. 11, the proposed HILS can be performed on the ground with or without a Helmholtz cage. First, the results obtained when the HILS was performed using the magnetic field of the original environment without generating a magnetic field from the Helmholtz cage show a different tendency

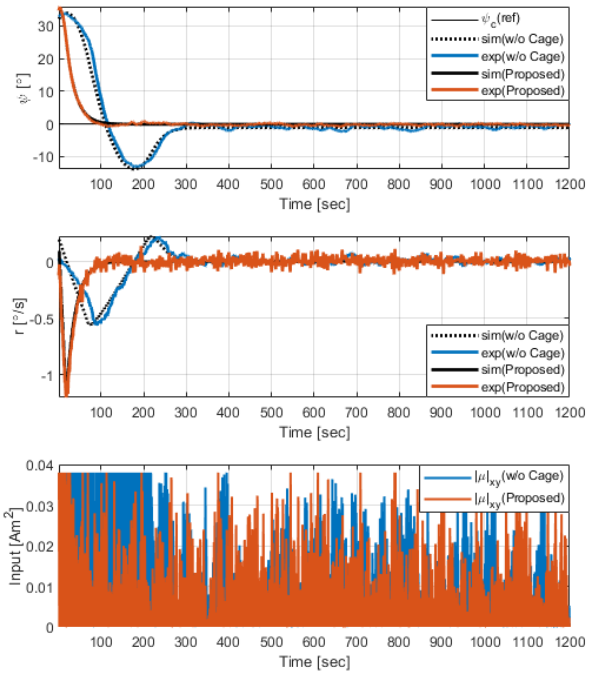

FIGURE 11. ADCS single-axis HILS experiment results. Comparison of simulation and experiment results when a magnetic field is generated by a Helmholtz cage and when it is not generated.

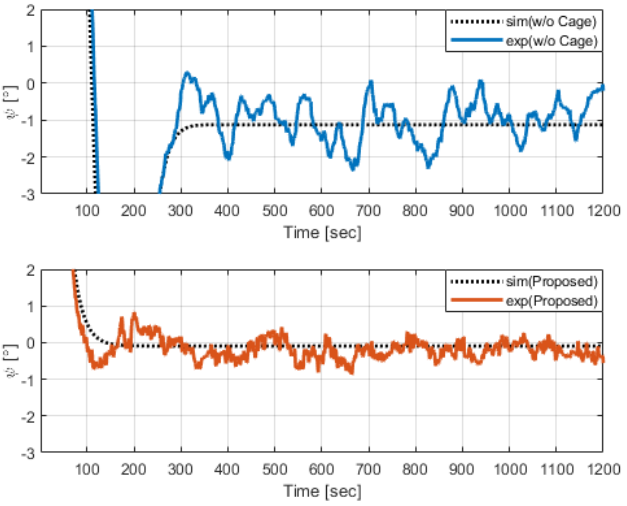

FIGURE 12. Expanding HILS experimental results. Comparison of simulation and experiment results when a magnetic field is not generated by a Helmholtz cage (upper) and when it is generated (lower).

compared to the simulation results. This difference exists because disturbance factors, which are the dominant factors with respect to the control torque, are not considered in the simulation and affect the ADCS performance. Moreover, even in the steady state, an error exists around a control input of 0°. In addition, the control input continuously used 100% of the input within the initial 300 s. In contrast, the proposed HILS results using the Helmholtz cage were consistent with the simulation and experimental results, because the dominant error element was removed from the Helmholtz cage by amplifying the control input torque from the magnetic field. The control input results also confirmed that less saturation occurred. The simulation results first confirm that a valid attitude is provided by the EKF. In other words, the statistical error reflected from the proposed time-varying bias compensation method of the magnetometer was well reflected in the EKF. In addition, effective control experiments on the ground are possible by reducing the disturbance and improving the torque performance of the magnetorquer by generating an amplified magnetic field from the Helmholtz cage.

To compare and analyze the performance, the results of enlarging the graph for the Euler angles are shown in Fig. 12. The convergence time is reduced to approximately half when the magnetic field is generated by the Helmholtz cage. Considering that the ADCS of a CubeSat is a very slow system, its performance can be quickly and accurately verified on the ground when a magnetic field is formed through a Helmholtz cage. In addition, the fast control performance indicates that the action of the control-torque input is remarkable. Thus, even the HILS experimental environment, which is vulnerable to external forces on the ground, can be interpreted as an environment in which the same performance as that of the simulation can be demonstrated. The results of comparing the performance by setting the control input to 0° are directly related to the ability of the CubeSat to perform missions in space. In Fig. 12, when the estimated Euler angle errors between 400 and 1200 s are defined as steady state, the RMS values are 1.17° and 0.32°, respectively, and the maximum values are 2.38° and 0.87°, respectively, showing performance improvement of 72% and 63%, respectively. In the case of the control input, the magnetic moment approaching the saturation was consumed in the results obtained without the Helmholtz cage up to the initial 100 s, whereas the proposed method shows performance improvement of 35% using an input of 64.2%. In the steady state, the ADCS performance is improved by 6%, from 44.5% to 41.1%. Thus, if the HILS method proposed in this paper is used, the performance results prove that the ADCS of the CubeSat can be efficiently verified using a simple device on the ground. In particular, focusing on the advantage that CubeSats are light and small, a simple space simulation environment was established by hanging them on a string. The time-varying bias compensation of the magnetic field was well reflected in the attitude determination in the proposed environment. In addition, the control input limit of the magnetorquer as the only mounted actuator, which is difficult to verify on the ground, was supplemented with a magnetic field generated by a Helmholtz cage. The results of the simulation and experiment matched. In addition, overall verification of the hardware and interface was performed by verifying the ADCS performance through actual experiments.

VI. CONCLUSION

This paper proposes a HILS method for a CubeSat platform, which developers can easily access. We developed a

HILS technique focused on CubeSat platform equipped with a magnetorquer and magnetometer. The time-varying bias of the magnetometer, which has been a chronic problem in CubeSats, was experimentally compensated, and based on this, the EKF was constructed for attitude determination. A 3-axis active control using an LQR controller was applied using the magnetorquer of CubeSat, and a single-axis based HILS technology using a Helmholtz cage was proposed to verify the CubeSat ADCS. This research has the following significance. First, a solution to the time-varying bias of a magnetometer that occurs on a very small platform, such as a CubeSat, was presented. In particular, because the hardware characteristics of the magnetometer are checked in advance before launch in the proposed approach and a solution is presented, HILS can be performed without the need for compensation using on-orbit data. The proposed algorithm was experimentally compensated for and reflected in the EKF, and its performance was demonstrated. In addition, a simple solution was proposed without introducing additional devices for the magnetometer, such as commercial boom products. Next, the active ADCS performance of CubeSat was verified on the ground in a simple and practical manner. Unlike the previous use of expensive devices, such as air bearings, to verify ADCSs on the ground, the ADCS performance could be verified very easily by simply hanging a CubeSat on a string and performing single-axis HILS. The uncertainty in the ground experiment was amplified by the control input of the magnetorquer through the magnetic field generated by the Helmholtz cage. In addition, considering the dominant disturbance torque of the modeled experimental environment, it was shown that the simulation and experiment yielded consistent results. Owing to the practicality and simplicity of the proposed method, it is anticipated that all developers who manufacture CubeSat platforms in the future will be able to perform ADCS verification reliably and improve the success rate.

ACKNOWLEDGMENT

The authors would like to thank the Institute of Engineering Research at Seoul National University for providing research facilities for this work.

REFERENCES

[1] S. Corpino and F. Stesina, "Verification of a CubeSat via hardware-in-the-loop simulation," *IEEE Trans. Aerosp. Electron. Syst.*, vol. 50, no. 4, pp. 2807–2818, Oct. 2014, doi: 10.1109/TAES.2014.130370.

[2] D. Y. Lee, H. Park, and J. W. Cutler, "Development of CubeSat attitude determination and control system with a hybrid control strategy and its simulator on SO(3)," in *Proc. 26th AAS/AIAA Spaceflight Mech. Meeting*, 2016. [Online]. Available: https://www.space-flight.org/docs/2016_winter/26thSFM_Program_FINAL.pdf

[3] M. S. Farissi, S. Carletta, A. Nascetti, and P. Teofilatto, "Implementation and hardware-in-the-loop simulation of a magnetic detumbling and pointing control based on three-axis magnetometer data," *Aerospace*, vol. 6, no. 12, p. 133, Dec. 2019, doi: 10.3390/aerospace6120133.

[4] J. Kiesbye, D. Messmann, M. Preisinger, G. Reina, D. Nagy, F. Schummer, M. Mostad, T. Kale, and M. Langer, "Hardware-in-the-loop and software-in-the-loop testing of the MOVE-II CubeSat," *Aerospace*, vol. 6, no. 12, p. 130, Dec. 2019, doi: 10.3390/aerospace6120130.

[5] A. Bahu and D. Modenini, "On-ground experimental verification of magnetic attitude control for nanosatellites," in *Proc. IEEE 8th Int. Workshop Metrology Aerosp. (MetroAeroSpace)*, Jun. 2021, pp. 568–573, doi: 10.1109/MetroAeroSpace51421.2021.9511720.

[6] D. Y. Lee, H. Park, M. Romano, and J. Cutler, "Development and experimental validation of a multi-algorithmic hybrid attitude determination and control system for a small satellite," *Aerosp. Sci. Technol.*, vol. 78, pp. 494–509, Jul. 2018, doi: 10.1016/j.ast.2018.04.040.

[7] G. Cervettini, S. Pastorelli, H. Park, D. Y. Lee, and M. Romano, "Development and experimentation of a CubeSat magnetic attitude control system testbed," *IEEE Trans. Aerosp. Electron. Syst.*, vol. 57, no. 2, pp. 1345–1350, Apr. 2021, doi: 10.1109/TAES.2020.3040032.

[8] G. Lavezzi, N. J. Stang, and M. Ciarcia, "Development of a low-cost satellite three-axis attitude simulator testbed," in *Proc. AIAA SCITECH Forum*, Jan. 2022, p. 2053, doi: 10.2514/6.2022-2053.

[9] N. Jovanovic, J. Pearce, and J. Praks, "Design and testing of a low-cost, open source, 3-D printed air-bearing-based attitude simulator for CubeSat satellites," *J. Small Satell. (JoSS)*, vol. 8, no. 2, pp. 859–880, 2019.

[10] D. Thomas, A. T. Wolosik, and J. Black, "CubeSat attitude control simulator design," in *Proc. AIAA Model. Simul. Technol. Conf.*, Jan. 2018, p. 1391, doi: 10.2514/6.2018-1391.

[11] M. Prinkey, "CubeSat attitude control testbed design: Merritt 4-coil per axis Helmholtz cage and spherical air bearing," in *Proc. AIAA Guid., Navigat., Control (GNC) Conf.*, Aug. 2013, pp. 1–12, doi: 10.2514/6.2013-4942.

[12] N. K. Ure, Y. B. Kaya, and G. Inalhan, "The development of a software and hardware-in-the-loop test system for ITU-PSAT II nano satellite ADCS," in *Proc. Aerosp. Conf.*, Mar. 2011, pp. 1–15, doi: 10.1109/AERO.2011.5747481.

[13] H. Woo, O. Rico, S. Chesi, and M. Romano, "CubeSat three axis simulator (CubeTAS)," in *Proc. AIAA Model. Simul. Technol. Conf.*, Aug. 2011, pp. 1–8, doi: 10.2514/6.2011-6271.

[14] L. Kruse, A. Plowcha, and J. M. Bradley, "Experimental testing and validation of cyber-physical coregulation of a CubeSat," in *Proc. AIAA SPACE Astronaut. Forum Expo.*, Sep. 2018, p. 5212, doi: 10.2514/6.2018-5212.

[15] J. Bouwmeester and J. Guo, "Survey of worldwide pico- and nanosatellite missions, distributions and subsystem technology," *Acta Astronautica*, vol. 67, nos. 7–8, pp. 854–862, Oct. 2010, doi: 10.1016/j.actaastro.2010.06.004.

[16] J. C. Springmann and J. W. Cutler, "Attitude-independent magnetometer calibration with time-varying bias," *J. Guid., Control, Dyn.*, vol. 35, no. 4, pp. 1080–1088, Jul. 2012, doi: 10.2514/1.56726.

[17] O.-J. Kim, H. Shim, S. Yu, Y. Bae, C. Kee, H. Kim, J. Lee, J. Han, S. Han, and Y. Choi, "In-orbit results and attitude analysis of the SNUGLITE cube-satellite," *Appl. Sci.*, vol. 10, no. 7, p. 2507, Apr. 2020, doi: 10.3390/app10072507.

[18] A. Chin, R. Coelho, R. Nugent, R. Munakata, and J. Puig-Suari, "CubeSat: The pico-satellite standard for research and education," in *Proc. AIAA SPACE Conf. Expo.*, Sep. 2008, pp. 1–11, doi: 10.2514/6.2008-7734.

[19] A. Poghosyan and A. Golkar, "CubeSat evolution: Analyzing CubeSat capabilities for conducting science missions," *Prog. Aerosp. Sci.*, vol. 88, pp. 59–83, Jan. 2017, doi: 10.1016/j.paerosci.2016.11.002.

[20] E. Gai, K. Daly, J. Harrison, and L. Lemos, "Star-sensor-based satellite attitude/attitude rate estimator," *J. Guid., Control, Dyn.*, vol. 8, no. 5, pp. 560–565, Sep. 1985, doi: 10.2514/3.56393.

[21] J. C. Springmann and J. W. Cutler, "Flight results of a low-cost attitude determination system," *Acta Astronautica*, vol. 99, pp. 201–214, Jun. 2014, doi: 10.1016/j.actaastro.2014.02.026.

[22] M. D. Shuster and S. D. Oh, "Three-axis attitude determination from vector observations," *J. Guid. Control*, vol. 4, no. 1, pp. 70–77, Jan. 1981, doi: 10.2514/3.19717.

[23] J. Jang, Y. Kim, H. No, S. Yu, O.-J. Kim, M. Choi, C. Kee, and S.-W. Seo, "Development and verification of LQG based attitude determination and control algorithm of cube-satellite 'SNUGLITE' using GPS and multiple sensors," in *Proc. 29th Int. Tech. Meeting Satell. Division Inst. Navigat.*, Nov. 2016, pp. 3731–3739, doi: 10.33012/2016.14645.

[24] V. G. Goecks, A. Probe, R. Woollands, J. E. Hurtado, and J. L. Junkins, "Low cost spacecraft attitude determination for CubeSat type missions," in *Proc. AAS Guid. Control Conf.*, 2016. [Online]. Available: https://www.researchgate.net/publication/333994148_Low_Cost_Spacecraft_Attitude_Determination_for_Cubesat_Type_Missions

[25] X. Han, X. J. Yang, and N. N. Abbas, "Design and simulation of attitude determination and control subsystem of CubeSat using extended Kalman filtering and linear quadratic gain controller," *Adv. Mater. Res.*, vols. 694–697, pp. 1582–1586, May 2013, doi: 10.4028/www.scientific.net/AMR.694-697.1582.
[26] A. Walker and M. Kumar, "CubeSat attitude determination using low-cost sensors and magnetic field time derivative," in *Proc. 55th AIAA Aerosp. Sci. Meeting*, Jan. 2017, p. 0166, doi: 10.2514/6.2017-0166.
[27] L. Baroni, "Attitude determination by unscented Kalman filter and solar panels as sun sensor," *Eur. Phys. J. Special Topics*, vol. 229, no. 8, pp. 1501–1506, May 2020, doi: 10.1140/epjst/e2020-900158-2.
[28] L. Baroni, "Kalman filter for attitude determination of a CubeSat using low-cost sensors," *Comput. Appl. Math.*, vol. 37, no. S1, pp. 72–83, Dec. 2018, doi: 10.1007/s40314-017-0502-5.
[29] S. Carletta, P. Teofilatto, and M. Farissi, "A magnetometer-only attitude determination strategy for small satellites: Design of the algorithm and hardware-in-the-loop testing," *Aerospace*, vol. 7, no. 1, p. 3, Jan. 2020, doi: 10.3390/aerospace7010003.
[30] E. Thébault, "International geomagnetic reference field: The 12th generation," *Earth, Planets Space*, vol. 67, no. 1, pp. 1–19, Dec. 2015, doi: 10.1186/s40623-015-0228-9.
[31] E. V. Pitjeva, "Modern numerical ephemerides of planets and the importance of ranging observations for their creation," *Celestial Mech. Dyn. Astron.*, vol. 80, no. 3/4, pp. 249–271, 2001, doi: 10.1023/A:1012289530641.
[32] F. L. Markley and J. L. Crassidis, *Fundamentals of Spacecraft Attitude Determination and Control*, vol. 1286. New York, NY, USA: Springer, 2014, doi: 10.1007/978-1-4939-0802-8.
[33] H. E. Soken, "A survey of calibration algorithms for small satellite magnetometers," *Measurement*, vol. 122, pp. 417–423, Jul. 2018, doi: 10.1016/j.measurement.2017.10.017.
[34] E. Kahr, N. Roth, O. Montenbruck, B. Risi, and R. E. Zee, "GPS relative navigation for the CanX-4 and CanX-5 formation-flying nanosatellites," *J. Spacecraft Rockets*, vol. 55, no. 6, pp. 1545–1558, Nov. 2018, doi: 10.2514/1.A34117.
[35] T. Inamori, R. Hamaguchi, K. Ozawa, P. Saisutjarit, N. Sako, and S. Nakasuka, "Online magnetometer calibration in consideration of geomagnetic anomalies using Kalman filters in nanosatellites and microsatellites," *J. Aerosp. Eng.*, vol. 29, no. 6, 2016, Art. no. 04016046, doi: 10.1061/(asce)as.1943-5525.0000612.
[36] H. E. Söken and C. Hajiyev, "UKF based in-flight calibration of magnetometers and rate gyros for pico satellite attitude determination," *Asian J. Control*, vol. 14, no. 3, pp. 707–715, May 2012, doi: 10.1002/asjc.368.
[37] C. Hajiyev, "Orbital calibration of microsatellite magnetometers using a linear Kalman filter," *Meas. Techn.*, vol. 58, no. 9, pp. 1037–1043, Dec. 2015, doi: 10.1007/s11018-015-0838-4.
[38] C. Hajiyev, "In-orbit magnetometer bias and scale factor calibration," *Int. J. Metrol. Quality Eng.*, vol. 7, no. 1, p. 104, 2016, doi: 10.1051/ijmqe/2016003.
[39] J. L. Crassidis, K.-L. Lai, and R. R. Harman, "Real-time attitude-independent three-axis magnetometer calibration," *J. Guid., Control, Dyn.*, vol. 28, no. 1, pp. 115–120, Jan. 2005, doi: 10.2514/1.6278.
[40] H. E. Soken, M. E. Çetin, and S. I. Sakai, "Attitude-independent magnetometer calibration for spinning spacecraft using quasi-measurements," in *Proc. AAS/AIAA Astrodyn. Spec. Conf.*, 2020.
[41] J. Guo, J. Zhang, C. Yue, and F. Wang, "Modeling of the CubeSat deployment and initial separation angular velocity estimation," *Aerosp. Sci. Technol.*, vol. 95, Dec. 2019, Art. no. 105477, doi: 10.1016/j.ast.2019.105477.
[42] J. Bouwmeester, A. Menicucci, and E. K. A. Gill, "Improving CubeSat reliability: Subsystem redundancy or improved testing?" *Rel. Eng. Syst. Saf.*, vol. 220, Apr. 2022, Art. no. 108288, doi: 10.1016/J.RESS.2021.108288.
[43] A. Wailand and R. Bauer, "Investigation of gain tuning and sensor noise for CubeSat B-dot detumbling and 3-axis PD magnetic attitude control," in *Proc. Can. Soc. Mech. Eng. Int. Congr.*, 2020, doi: 10.32393/csme.2020.1156.
[44] R. Wisniewski, "Linear time-varying approach to satellite attitude control using only electromagnetic actuation," *J. Guid., Control, Dyn.*, vol. 23, no. 4, pp. 640–647, Jul. 2000, doi: 10.2514/2.4609.
[45] M. L. Psiaki, "Magnetic torquer attitude control via asymptotic periodic linear quadratic regulation," *J. Guid., Control, Dyn.*, vol. 24, no. 2, pp. 386–394, Mar. 2001, doi: 10.2514/2.4723.
[46] A. R. Walker, P. T. Putman, and K. Cohen, "Solely magnetic genetic/fuzzy-attitude-control algorithm for a CubeSat," *J. Spacecraft Rockets*, vol. 52, no. 6, pp. 1627–1639, Nov. 2015, doi: 10.2514/1.A33294.
[47] J. Kim, Y. Jung, and H. Bang, "Linear time-varying model predictive control of magnetically actuated satellites in elliptic orbits," *Acta Astronautica*, vol. 151, pp. 791–804, Oct. 2018, doi: 10.1016/j.actaastro.2018.07.029.
[48] P. Wang and Y. B. Shtessel, "Satellite attitude control using only magnetorquers," in *Proc. Amer. Control Conf.*, 1998, pp. 222–226, doi: 10.1109/ACC.1998.694663.
[49] D. M. Torczynski, R. Amini, and P. Massioni, "Magnetorquer based attitude control for a nanosatellite testplatform," in *Proc. AIAA Infotech Aerospace*, 2010, p. 3511, doi: 10.2514/6.2010-3511.
[50] I. Ofodile, J. Kutt, J. Kivastik, M. K. Nigol, A. Parelo, E. Ilbis, H. Ehrpais, and A. Slavinskis, "ESTCube-2 attitude determination and control: Step towards interplanetary CubeSats," in *Proc. IEEE Aerosp. Conf.*, Mar. 2019, pp. 1–12, doi: 10.1109/AERO.2019.8741929.
[51] S. Kukreti, A. Walker, P. Putman, and K. Cohen, "Genetic algorithm based LQR for attitude control of a magnetically actuated CubeSat," in *Proc. AIAA Infotech Aerospace*, 2015, p. 0886, doi: 10.2514/6.2015-0886.
[52] F. Primdahl, "Temperature compensation of fluxgate magnetometers," *IEEE Trans. Magn.*, vol. M-6, no. 4, pp. 819–822, Dec. 1970, doi: 10.1109/TMAG.1970.1066971.
[53] J. P. Mason, B. Lamprecht, T. N. Woods, and C. Downs, "CubeSat on-orbit temperature comparison to thermal-balance-tuned-model predictions," *J. Thermophys. Heat Transf.*, vol. 32, no. 1, pp. 237–255, Jan. 2018, doi: 10.2514/1.T5169.
[54] D. Gebre-Egziabher, G. H. Elkaim, J. David Powell, and B. W. Parkinson, "Calibration of strapdown magnetometers in magnetic field domain," *J. Aerosp. Eng.*, vol. 19, no. 2, pp. 87–102, 2006, doi: 10.1061/(asce)0893-1321(2006)19:2(87).
[55] H. S. Ousaloo, G. Sharifi, J. Mahdian, and M. T. Nodeh, "Complete calibration of three-axis strapdown magnetometer in mounting frame," *IEEE Sensors J.*, vol. 17, no. 23, pp. 7886–7893, Dec. 2017, doi: 10.1109/JSEN.2017.2766200.
[56] E. J. Lefferts, F. L. Markley, and M. D. Shuster, "Kalman filtering for spacecraft attitude estimation," *J. Guid., Control, Dyn.*, vol. 5, no. 5, pp. 417–429, Sep. 1982, doi: 10.2514/3.56190.
[57] H. Shim, "HILS verification of low Earth orbit cube-satellite attitude determination and control system using helmholtz cage," M.S. thesis, School Mech. Aerosp. Eng., Seoul Nat. Univ., Seoul, South Korea, 2019.
[58] M. Choi, J. Jang, S. Yu, O.-J. Kim, H. Shim, and C. Kee, "Single-axis hardware in the loop experiment verification of ADCS for low Earth orbit cube-satellite," *J. Positioning, Navigat., Timing*, vol. 6, no. 4, pp. 195–203, 2017, doi: 10.11003/JPNT.2017.6.4.195.
[59] M. J. Sidi, *Spacecraft Dynamics and Control: A Practical Engineering Approach*, vol. 7. Cambridge, U.K.: Cambridge Univ. Press, 1997, doi: 10.1017/CBO9780511815652.
[60] A. E. Bryson, *Control of Spacecraft and Aircraft*, vol. 41. Princeton, NJ, USA: Princeton Univ. Press, 1993, doi: 10.1515/9781400880034.
[61] I. Gaponov, D. Popov, and J. Ryu, "Twisted string actuation systems: A study of the mathematical model and a comparison of twisted strings," *IEEE/ASME Trans. Mechatronics*, vol. 19, no. 4, pp. 1331–1342, Aug. 2014, doi: 10.1109/TMECH.2013.2280964.

HANJOON SHIM received the B.S. degree in mechanical and control engineering from Handong Global University and the M.S. degree from the School of Mechanical and Aerospace Engineering, Seoul National University. He is currently pursuing the Ph.D. degree with the GNSS Laboratory, Department of Aerospace Engineering, Seoul National University. His research interests include the development of autonomous guidance, navigation, and control systems for spacecraft, CubeSat technology, attitude determination and control, GPS RTK relative navigation, and hardware-in-the-loop simulation for CubeSat projects. With a passion for advancing the field of space exploration, his current research interests include the advancement of CubeSat technology and the development of advanced autonomous GN&C systems for spacecraft.

O-JONG KIM received the B.S., master's, and Ph.D. degrees from Seoul National University. He was with System LSI Business of Samsung Electronics. He is currently an Assistant Professor with the Department of Aerospace Engineering, Sejong University, South Korea. His current research interests include alternative PNT, indoor navigation, cycle ambiguity resolution, and space technologies, such as space GNSS receivers and nano-satellite platforms.

MINHUCK PARK received the B.S., M.S., and Ph.D. degrees from the School of Mechanical and Aerospace Engineering, Seoul National University, Seoul, South Korea, in 2015, 2017, and 2022, respectively. He is currently a Senior Researcher with Danam Systems Corporation Ltd. His current research interests include GNSS receivers and spoofing and GPS/INS integrated navigation systems.

MINKYU CHOI received the B.S. degree from Handong Global University and the M.S. degree from the School of Mechanical and Aerospace Engineering, Seoul National University, South Korea. His current research interests include sensor integration and CubeSat attitude determination and control systems.

CHANGDON KEE (Member, IEEE) received the B.S. and M.S. degrees from Seoul National University (SNU), South Korea, and the Ph.D. degree from Stanford University. He was a Technical Advisor of the Federal Aviation Administration (FAA) on the Wide Area Augmentation System (WAAS), in 1994. He was the President of the Korean Institute of Navigation. He is currently a Professor with the Department of Aerospace Engineering, SNU, and supervises the SNU GNSS Laboratory (SNUGL, http://gnss.snu.ac.kr). He is also a Technical Advisor of the Korea Civil Aviation Safety Authority (KCASA) and the Ministry of Public Administration and Security (MOPAS). He has more than 20 years of GNSS and flight control research experience.